Medium Diagnostics for a 10-kW cw HF Chemical Laser

Munson A. Kwok,* Robert R. Giedt,† and Robert L. Varwig‡
The Aerospace Corp., El Segundo, Calif.

The supersonic free jets of an arc-driven 10-kW cw HF chemical laser were studied for fixed-flow conditions with and without lasing. A spatially, spectrally, rapidly scanning spectrograph and a spatially scanning stagnation and static pressure probe were used in the diagnosis. The average static temperature and average HF(3) populations were deduced for a very large number of positions in the flow. Salient results include the capability of evaluating the uniformity of reaction in the jet, especially along the cavity axis near the nozzle exit plane, and a qualitative evaluation of the degree of consumption of lasant reactant in the cavity region. A significant local cooling effect resulting from power extraction was observed. Spatial scans of stagnation and static pressures were made for the zero-power case, and Mach numbers and local mass densities were deduced.

Nomenclature

M	= Mach number
$\dot{m}_i$	= mass flow rate of species i ($g\text{-sec}^{-1}$)
$\bar{N}_3L$	= average number density along line of sight of HF(3) ($No.\text{-cm}^{-2}$)
P_{LP}	= laser plenum pressure (psia)
P_{LC}	= laser chamber pressure (Torr)
p	= static pressure in jet (Torr)
p_t	= stagnation pressure in jet (Torr)
$\dot{Q}_{CHEM}$	= heat transferred to jet from chemistry (W)
R_i	= gas constant of species i ($J-K^{-1}-gm^{-1}$)
T	= static temperature (K)
T_0	= stagnation temperature (K)
T_R	= average rotational temperature (K)
W	= closed-cavity laser power (kW)
W_i	= molecular weight of species ($g\text{-mol}^{-1}$)
x	= jet coordinate in flow direction (cm)
y	= jet coordinate along spectroscopic line of sight (cm)
z	= jet coordinate transverse to flow direction (cm)
α	= F_2 dissociation $[F]/([F]+2[F_2])$
β	= plenum dilution $[He]/([F]+[F_2])$
γ	= ratio of specific heats
ρ	= gas density ($g\text{-cm}^{-3}$)

Introduction

THE characterization of the performance of a cw HF chemical laser requires an understanding of the behavior of the lasing medium with and without power extraction. In the supersonic diffusion laser,[1] the lasing medium is a low-pressure supersonic free jet array in which HF(v) is highly diluted. Therefore, a complete understanding of the medium requires a detailed determination of certain local properties. In this study, time-averaged results obtained from optical diagnostics are stressed. The system detects HF(3) spontaneous emission.[2] The principal measurements are static temperature and HF(3) average density. Stagnation and static pressures that yield Mach number information and also permit the calculation of local mass densities are reported. The spatial variations in static temperature and HF(3) density provide information on the uniformity of reaction along the cavity axis. The completeness of reaction within the cavity zone is estimated from the static temperature measurements. The effect of power extraction on these measured parameters is examined.

Received June 23, 1975; revision received April 5, 1976. Research supported by the Air Force Weapons Lab. of the Dept. of Defense under U.S. Air Force Space and Missiles Systems Organization (SAMSO) Contract F04701-75-C-0076 is described. The authors acknowledge extensive help of W. R. Warren, The Aerospace Corp.; Lt. Col. R. Oglukian and Maj. R. Klopotek, AFWL; and S. Gunn and associates, Rockwell International Corp. The assistance of the Aerospace MESA staff, especially W. Gaskill and R. Harwell, J. McKay, and R. H. Ueunten, The Aerospace Corp., and the AFRPL organization is also appreciated.

Index categories: Reactive Flows; Lasers; Supersonic and Hypersonic Flow.

*Member of the Technical Staff, Aerophysics Lab. Member AIAA.
†Manager, Test Operations, Aerophysics Lab.
‡Staff Scientist, Aerophysics Lab. Member AIAA.

Experiments

The static temperature of the supersonic free jet of the lasing medium is measured with the spatially, spectrally, rapidly scanning spectrograph system.[2] Average number densities of HF(3) along the line of sight are also deduced. The spectroscopic technique was chosen because the medium is highly corrosive, and a conventional temperature probe cannot survive in a large F or F_2 flow at high stagnation temperatures. The optical method has the advantage that the medium is not disturbed by the measurement, and therefore, the medium can be observed with or without laser cavity for comparison. The HF 3→0 vibrational-rotational P-branch was selected for several reasons. With low Einstein transition probabilities applicable, the observed medium is optically thin even at large HF densities or with large amounts of recirculating HF(0). The use of a second overtone negates concern with atmospheric absorptions. For rapid scanning, photomultiplier tube detectors dictate the use of the second or higher overtone; for the largest signal, the HF(3) level is used. The first five P-branch lines are used because they can be treated as isolated spectral lines without interference from the 4→1 band.

The grating spectrograph system is shown in Fig. 1. It has been discussed previously.[2,3] A rapid spectral scan over 20 nm centered at wavelength 880 nm requires 20 msec; the scan period is 0.1 sec. Geometric axes can be defined with the origin at the center of the nozzle exit plane and with x-y-z axes; the z axis parallels the laser cavity centerline. Translation of spectrographic field of view (FOV) along z is accomplished by the slow pivoting mirror movement; along x, it is accomplished by the motion of the MESA chamber and spectrograph structure relative to the nozzle array. The position of the FOV in the laser medium is determined by two potentiometer linkages to the moving parts; spatial calibration is performed by means of a two-ended He-Ne 633-nm laser located inside the spectrograph on the optical centerline. A double 45-deg mirror system reorients the vertical entrance slit parallel to the x axis. The effective solid angle of the system is 2.3×10^{-3} steradians An absolute intensity calibration of the system is performed.

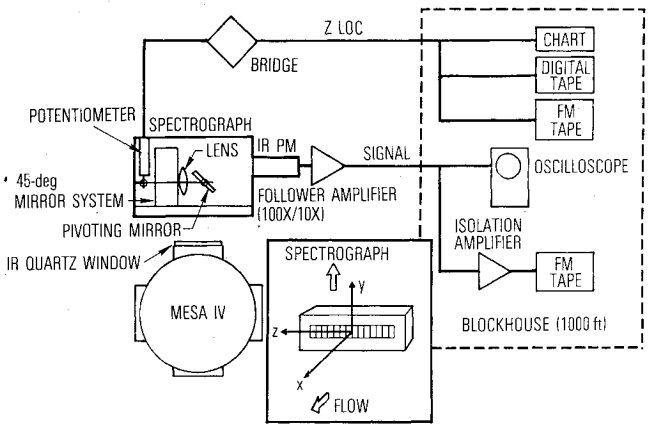

Fig. 1 Spectrograph experiment. The 12-port cylindrical laser chamber is schematically depicted in end view looking along x with the experiment on top. The insert shows the x-y-z coordinate system. The nozzle and cavity systems are described in the text.

Mach numbers are estimated from photographs of angles of shocks emanating from the leading edge of a water-cooled, 24-deg copper wedge located at $x=12.7$ cm and $z=0$ before chamber movement. This edge is therefore 2.5 cm downstream of the cavity.

Pitot and static pressures are measured in the supersonic free jet by means of the typical pitot static probe. This consists of a flat plate wedge with a pitot tube appendage on the probe centerline below the flat plate surface. The body of the probe is constructed of copper and is water cooled. Static pressure is sensed through a 0.0396-cm-diam port 0.51 cm aft of the leading edge on the flat plate by one of two strain-gage pressure transducers within the probe body. Since the gage is close to the port, the response time is minimized. The 0.0127-cm-thick, 0.0635-cm-diam copper pitot tube protrudes from the wedge even with the leading edge. Because the probe surface is cooled, because the freestream unit Reynolds number is high ($Re\simeq 2\times 10^5$/ft), and because the Mach number is moderate, the induced pressure and flow deflection produced by the probe can be neglected. To determine any effect of the proximity of the wedge edge on the pitot pressure, the pressure measured by the pitot static probe is compared with that measured by a previously developed[4] single pitot pressure probe model. For nearly identical flows, the pitot pressures measured by the two probes differed by only 0.90%; hence, no wedge effect exists. Probe z-transverse speed is 0.064 cm-sec^{-1} for reasonable resolution.

Theory

The formulae for deducing T_R and $\bar{N}_3L$ have previously been given for the case when T_R is spatially uniform within the optical volume.[2,5] Success in optically determining the static temperature depends on the assumptions that the rotational levels of a given vibrational state are equilibrated, and that the rotational and translational degrees of freedom in HF are equilibrated with themselves and with the bath molecules. For the present flow rates, pressures, and estimated temperatures in the jet, at least 50 to 100 collisions can occur in a 2-mm-diam spherical volume, even in the direction of the supersonic stream in a 10-Torr, 400-K, Mach 4 flow. The bath molecules are predominantly H_2 or He on a 1:1 ratio. Recent work[6] shows that equilibration occurs for HF(2) at rotational quantum numbers $J\leq 4$ within 30 collisions in an H_2 bath. The number of collisions is adequate to achieve equilibration for $J\leq 4$ even if the observed HF(v) is the newly reacted product. The emission consists of isolated spectral lines and can be considered to be emanating from an optically thin medium. For these estimated HF concentrations, the Doppler width is 3×10^{-3} nm, which is considerably smaller than the instrument width, 1.75 nm. Therefore, the peak signal observed when the instrument is set at the center frequency of the line is proportional to the integrated power from the spectral line shape. This power is from intensities that have also been integrated over the optical volume defined by the optics, apertures, and entrance slit. T_R is deduced from a straight-line semilogarithmic plot of adjusted relative intensity vs rotational energy spacing of HF(3). Optical volume integrations for the case when T is not uniform in the volume indicate that T_R is at worst an upper bound to spatially averaged T, and that 30% fluctuations in T lead to an apparent T_R 10% larger than spatially averaged static temperature (see Appendix.)

Deductions of Mach number and gas velocity require that γ and W_i of the gas be estimated. Because of the high dilutions of these flows in He and H_2, the situation is simplified. These two quantities are best known at the nozzle exit plane and at some great distance downstream in the free jet when the fuel is well mixed with the other species. In the oxidizer nozzle exit, γ and W_i are specified by the flow rates and the estimated F_2 dissociation. At the downstream position, the additional information on fuel flow rate and the additional assumptions of complete combustion to HF and total mixing are used. Because of the great dilutions, any errors in estimating oxidizer or product species are not serious. With the wedge, Mach number is found with the usual relation involving M with γ, the shock angle, and the wedge half angle. With the pressure probes, a Rayleigh formula can be used, relating ratio of pitot and static pressures to γ and M; alternatively, at the nozzle exit, the ratio of nozzle plenum and pitot pressures can be used.

The study of the thermal effects depend on the relation at any local jet position:

$$T=(T_0)\{1+[(\gamma-1)M^2/2]\}^{-1} \tag{1}$$

T_0 is changed along a streamline by nonadiabatic phenomena. In a jet control volume, the total rate of increase of stagnation enthalpy equals the heat transferred to the volume; at a downstream position 2,

$$T_{02}=\{[\dot{m}R\gamma^{-1}(\gamma-1)]_2\}^{-1}\{[\dot{m}R\gamma^{-1}(\gamma-1)T_0]_{LP} + [\dot{m}R\gamma^{-1}(\gamma-1)T_0]_{\text{FUEL}}+\dot{Q}_{\text{CHEM}}-10^3W\} \tag{2}$$

The first two r.h.s. terms are stagnation enthalpies of gases from the oxidizer nozzles and fuel, respectively. The third term is the heat generated from the HF-producing chemical reactions; $\dot{Q}_{\text{CHEM}}$ equals $(14224-7255\alpha)\dot{m}_{F_2}$.

The Laser

The cw HF laser used in these tests is a supersonic diffusion laser that uses arc-heated He to dissociate the F_2 oxidizer. The laser is located at the Rocket Propulsion Lab. so that large flow rates of F_2 can be handled. The fuel used is H_2, and the instrumentation is remotely controlled from a blockhouse. The He is heated in an arc plenum in a dc arc device and is injected into the nozzle plenum to mix with F_2 and additional He. The F, F_2, and He are then supersonically expanded in one of two possible cooled nozzle arrays into a laser chamber kept at low pressures such that a supersonic free jet system is formed. H_2 is injected from secondary nozzles in the arrays on the exit plane and mixes with the oxidizer flow. The predominant exothermic reaction

$$F+H_2\rightarrow HF(v)+H \tag{3}$$

occurs, producing the lasing species. The jets are then exhausted through heat exchangers and a straight 60-cm-diam pipe to a high-capacity steam injector system capable of low-Torr operation for an extended time interval.

The two nozzle arrays consist of axisymmetric and two-dimensional slit nozzles. The axisymmetric pattern is 3.8 cm

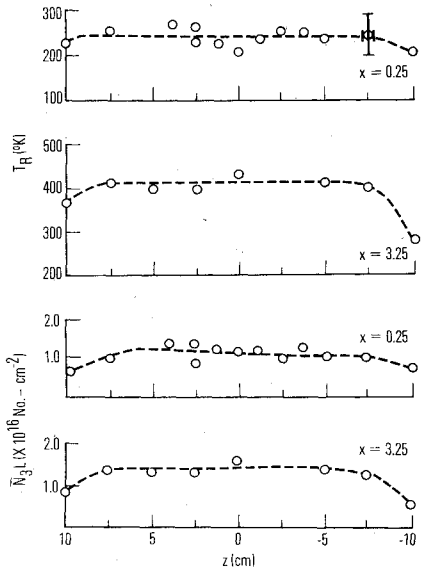

Fig. 2 Plots of rotational temperature T_R and HF(3) number density $\bar{N}_3L$ vs transverse coordinate for slit array. Test 418 (power-off). Specific test conditions are given in Table 1. Transverse scans were performed at the following x stations: 0.635 (0.25 in.), 1.905, 3.175, 5.715, and 8.255 (3.25 in.) cm. Two stations are shown. Optical spatial resolution is $\Delta x \times \Delta z = 0.89$ cm $\times$ 0.23 cm.

high by 22.8 cm long in the z direction, the direction of the cavity axis. The pattern consists of 655 conical oxidizer nozzles in 69 vertical columns with alternate nine- and ten-nozzle columns. Each nozzle has a nominal exit-to-throat area ratio of 18 and an exit area 0.25 cm in diameter. Concentrically located, a fuel nozzle surrounds each oxidizer nozzle. The slit array consists of 50 oxidizer nozzles with a total area of 1.90 by 22.8 cm. The nominal area ratio is 30. The oxidizer nozzles alternate with 51 narrower fuel nozzles. The relative effective "wetted" perimeter between oxidizer and fuel for the axisymmetric nozzle bank is 5.4 times that of the slit nozzle.

The laser cavity consists of 10.2-cm-square gold-coated mirrors over-coated with MgF_2 in a stable configuration. One mirror is flat; the other nominally has a 304-cm radius of curvature. The cavity is 56 cm long. Power measurements are made by means of the closed-cavity technique, which involves the calorimetric measurement of photon energy transferred to the mirror. Mirror tilt can be remotely controlled to move the cavity axis in the x or y direction. The entire mirror system can be translated in the x direction without tilt to map the gain zone by the same movement of the laser chamber that moves the spectrograph system.

Results and Discussion

Typical spatial distributions in z of T_R and $\bar{N}_3L$ for the slit nozzle are shown in Fig. 2; the typical optical resolution $\Delta x \times \Delta z$ at $y = 0$ is given. Flow conditions are given in Table 1. The conditions chosen for study approximate those for optimum laser power. Test points 414-16 and 417-03 were laser power-on tests with the axisymmetric array. Test points 413-36 and 419-02 were the power-on runs with the slit array, whereas 418 was the corresponding laser power-off case with virtually identical flow conditions. To allow rapid spatial scanning and to maintain an effective minimum signal-to-noise ratio of ~10, no attempt has been made to resolve individual flamesheets in these studies. The uncertainties in T_R are estimated to be ±50K with 95% confidence for most points and for some low-level, but readable, intensity signals as great as ±100K. The uncertainties in relative $\bar{N}_3L$ from place to place in the flow are ~30% of value. The uncertainty in an absolute number density is estimated to be a factor of 2 at best since an absolute radiance calibration and a precise definition of the optical geometry must be made. These results from the data reduction of the oscilloscope pictures, which are the average of ten spectral scans, agree with a more detailed single-scan analysis.[3] With the scanning mirror in motion, the effective movement in z for the ten scans is 0.5 cm.

T_R and $\bar{N}_3L$ exhibit jet transverse uniformity in z over 18 of 23 cm. This result appears to be independent of nozzle bank and laser power conditions and is obviously a reflection of the uniform plenum distribution of F and F_2 because T_R depends on heat flux from exothermic reactions [Eqs. (1) and (2)]; $\bar{N}_3L$ can be shown in an excess fuel condition to be proportional to initial F plus F_2 densities at nozzle exits. Near the edges of the jet, the lower T_R and $\bar{N}_3L$ suggest a decrease in the oxidizer concentration near the plenum walls. The same transversely uniform properties have been observed at several downstream x stations (Fig. 2) in the power-off condition. A similar uniformity trend was evident in the pressure measurements.

Spatial variations in x are shown in Fig. 3 for power-off (Test 418) and power-on (Test 419-02) conditions in the slit nozzle. These variations are all at $z = 0$ although similar plots at other z points can be constructed from the data. They reflect the cumulative effects of heat release during combustion, weak oblique shock structure, expansion waves, and power extraction. The spatial resolution (0.2 × 0.9 cm) is sufficiently low such that the measured parameters are spatially averaged over one oxidizer jet in the z direction. However, the average is weighted where HF(3) is present, i.e., in the flame regions. (Photographs show that jet expansion is considerable along the y axis since the jet is substantially underexpanded.) Similar results are obtained in axisymmetric Test 417-03 (Table 1).

A comparison of power-off and power-on conditions (Fig. 3) suggests that HF(3) is affected by the photon flux at small x and that a "cooling effect" is manifested. In the power-on case, the spectrographic optical volume is always within the laser cavity and 0.63 cm from the upstream cavity edge. For Test 418, M can be taken as the average (= 2.3) of those for 413 and 419 with less than 3% error because of the similar flow conditions; reduction of the power in 413-36 by more than a factor of 5, as a result of cavity mirror rotation, produced no change in M at $x = 12.7$cm. This is consistent with present laser power extracted being ~3% of the total jet energy in terms of stagnation enthalpy. Therefore, the

Table 1 Operating conditions

Test	Flow rates (g-sec^{-1})			P_{LP}	T_{LP}	α	β	P_{LC}	M	W
	He	F_2	H_2	(psia)	(K)			(Torr)	$x = 12.7$ cm	(kW)
					Axisymmetric array					
414-16	23.8	15.1	14.8	70	1630	0.95	14.8	2.2	...	10.7
417-03	28.7	14.8	14.7	81	1330	0.65	18.4	1.7	...	11.6
					Slit array					
413-36	20.0	15.0	10.9	90	1440	0.76	12.6	2.4	2.2	12.4
418	19.9	15.3	11.0	92	1373	0.64	12.3	3.3	...	0
419-02	20.0	14.8	10.9	90	1280	0.48	12.7	2.3	2.4	12.4

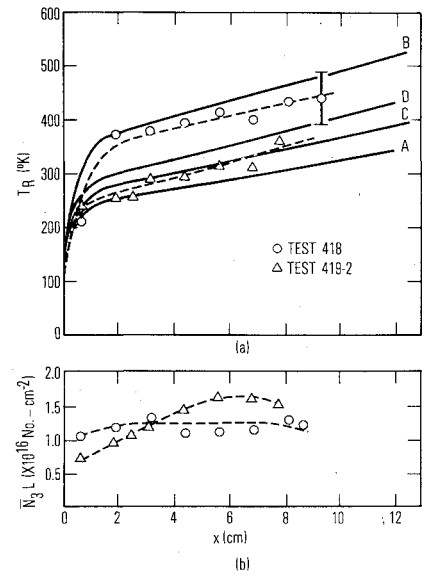

Fig. 3 Plots of a) rotational temperature T_R and b) HF(3) number density $\bar{N}_3L$ vs flow coordinate x for slit nozzle array. Tests 418 (power off) and 419-02 (power on). $z=0$. Optical spatial resolution $\Delta x \times \Delta z = 0.89$ cm $\times 0.20$ cm. Model curves are from jet calorimetry. Curve A: Fully mixed, no reaction. Curve B: Complete mixing and reaction, vibrational-translational transfer. Curve C: Complete mixing and reaction, no vibrational-translational transfer. Curve D: Complete mixing and reaction, $H+F_2$ with full heat release to flow, $F+H_2$ product HF with no vibrational-translational transfer.

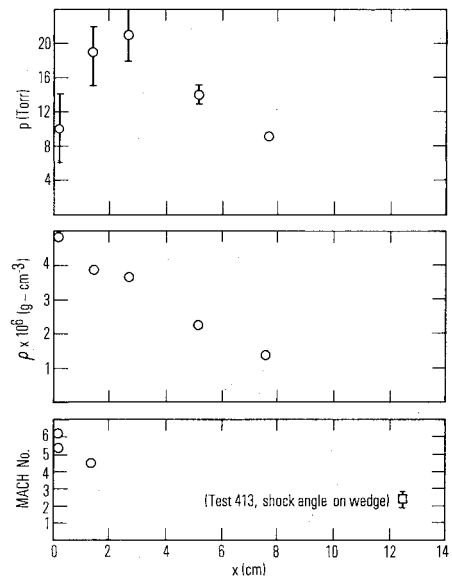

Fig. 4 Axial variation in supersonic jet of static pressure p, mass density ρ, and Mach number M. Slit nozzle array. Test 418. $z=0$.

gasdynamics of the flow should be affected little by the extraction. This fact is also reflected in the stagnation temperature calculation Eq. (2) for power-off (Test 418) and power-on conditions (419-2) (Table 2). The slight reduction in T_0 in 419-2 as a result of power extraction is compensated for by the slight reduction in α, yielding more exothermicity from $H+F_2$. Since the Mach numbers change little in these cases, T changes by 5%, and therefore, the 30% or 100K change in observed static temperature cannot be attributed to the gross effects of power extraction.

Curves computed from Eqs. (1) and (2) and from M (Fig. 4) are used to explain the 100K difference. These curves are generated by the use of a control volume that encompasses all the gas flow in the supersonic jet arrays. The upstream plane of the volume is the exit plane, and the downstream plane is station 2 at which M is recorded. Completeness in mixing and combustion is obviously a better assumption for large x. However, the assumption is probably locally valid in the regions of strong HF(3) emission, i.e., the reaction zone where mixing and reaction are largely completed. In any case, calculated T is a realistic upper limit for T_R. In Fig. 3, the experimental observations are indeed between Curve B (completed mixing and reaction) and Curve A (completed mixing with no reaction). The agreement of Curve B with the power-off points is good. The uncertainty in measuring wedge Mach numbers is 5%, which leads to a corresponding uncertainty in a calculated T of 5% or ± 30 K.

Curve C represents the heat transfer to a jet at 418 conditions from initial translational energy produced by reactions $F+H_2$ and $H+F_2$. In the former reaction,[7] only 30% of the exothermic energy becomes translational energy; in the latter,[8] 50% does. A static temperature discrepancy of exactly the correct magnitude is generated between Curves B and C, which implies that inside the upstream cavity edge the internal vibrational and rotational energies of local HF(v) are nearly completely extracted as photons. Because of the highly coupled, stable, closed-cavity configuration, it is probable that many of these photons are reabsorbed downstream, saturating the medium and equalizing the spatially inhomogeneous number densities. This reabsorbed photon energy ultimately must become translational energy through collisional deactivation. We anticipate that T measured at the downstream cavity edge would approach T_R observed at that x for zero-power conditions, and no discrepancy in temperature would be found. Therefore, the observed temperature difference is a local effect.

T calculated at 12.7 cm is a good basis of comparison for the completeness of reaction in the case of free jets with monotonically increasing T. In Table 2, some comparisons of T_R at $x=2.54$ cm and T at 12.7 cm are made. It can be seen from the larger T_R/T ratio that the axisymmetric bank is a faster reacting array (and therefore faster mixing). Since the mixing processes for the two arrays are similar, this is consistent with the greater wetted perimeter in the axisymmetric array. The HF pumping reactions and the net deactivations are accelerated. For approximately the same flow conditions, a shorter gain zone is expected and observed, since an x variation of the cavity shows the power zone length in x to be half that for the slit bank.

Pitot- and static-pressure measurements were made in Test 418 on nozzles in a plane 0.13 cm downstream of the exit plane and at stations $x=1.40$, 2.67, and 7.75 cm. Typical measurements on the centerline of these nozzles are listed in Table 3 for station 0.13. The pitot probe burned or melted off after station 1.40 so that only static pressure was recorded for stations 2.67, 5.09, and 7.75. In Table 3, the Mach number is

Table 2 Calorimetry

Test	$\dot{Q}_{CHEM}/[\dot{m}R(\gamma-1)\gamma^{-1}]_2$ (K)	$W/[\dot{m}R(\gamma-1)\gamma^{-1}]_2$ (K)	T_0 $x=12.7$ (K)	M $x=12.7$	T $x=12.7$ (K)	T_R $x=2.54$ (K)	T_R/T
414-19[a]	347	25	1172	2.9	378	330	0.87
418[b]	553	0	1211	(2.3)	528	370	0.70
419-02[b]	553	43	1209	2.4	500	252	0.50

[a]Test 414-19; axisymmetric array. [b]Test 418 and 419-02: slit array.

Table 3 Pitot and static pressures at nozzle exit station
Test 418, $P_{LP} = 95$ psi

Nozzle no.	p_t (Torr)	p_t/P_{LP}	M	p (Torr)	p/p_t	M
20	360	0.074	6.4	10.6	0.0294	4.8
21	450	0.091	5.9	10.0	0.0222	5.5
22	410	0.083	6.1	10.2	0.0248	5.2
23	350	0.072	6.5	9.4	0.0268	5.0
24	420	0.086	6.1	9.5	0.0226	5.5
25	430	0.087	6.0	10.0	0.0232	5.4
26	480	0.097	5.8	9.5	0.0198	5.8
average			6.1 ± 0.3			5.5 ± 0.3

calculated on the basis of either the measured pitot and plenum pressures or the measured pitot and static pressures by the use of the appropriate Rayleigh formula for seven centrally located nozzles. M is 6.1 ± 0.3 (at the nozzle exit) when calculated from the former method to a 90% confidence interval, and is 5.5 ± 0.3 when calculated from the latter. The differing results are associated with difficulty in reading the pitot pressure. There are both a probe effect and shock structure in the flow that influence the pitot pressure observed. The probe effect is a small asymmetry in the scan caused by the trapping of nozzle wall boundary layer between wedge and pitot probe when the probe is very close to the nozzle exit plane, thereby making the observed pitot pressure higher on the side of the probe where the wedge wall is located. The effect disappears as soon as the probe is moved aft of the nozzle exit plane. The shock structure is caused by a "displacement wedge" effect resulting from the $F+H_2$ reaction beginning just downstream of the nozzle exit.[9]§ The effect may also contribute to nozzle wall separation and attendant separation shock waves.

The Mach number calculated from the pitot- and static-pressure measurements at station 1.40 is 4.4 ± 0.3, although there is considerable variation in the pitot and static pressures measured. Variations in pitot pressures are assumed to be real and are probably the result of variations in nozzle conditions and mixing and reaction in the flowfield. The scale of the pitot probe is small enough (between 0.038 cm and 0.086 cm) to exhibit much of the flow structure. However, for the static pressure, shock waves in the flow reflecting from the flat plate surface where the pressure is sensed can cause pressures that are higher than those in the flow behind the shock. The static pressure measured in this region must be considered to have an uncertainty of $\pm 20\%$, which must be reflected in the uncertainty of the flow Mach number. As expected, the static pressure profile observed begins to smooth out at the downstream locations by the reduction in variation from the mean. The axial variations of static pressure and Mach number are plotted in Fig. 4 and are found to be large at small x. From the measured static pressure and the temperature obtained from rotational temperature data on the same test, density in the flowfield was calculated (Fig. 4). Downstream, the average W_i was determined with all gases input to the plenum and at the nozzle exit assumed to be well mixed. At the nozzle exit station, W_i was taken to be that of the plenum gas. Since the centerline static pressure is representative of the flame zone pressures in these diluted flows, the deduced mass density is an average density in the flame zone at given x. A local gas velocity can also be computed.

The observed trends for local T, p, M, and ρ are considered to be representative of the free, underexpanded, supersonic reacting jet array. The density reflects the static pressure that is to be expected since the temperature, after a sharp rise close to the nozzle exit, is nearly steady. The Mach number close to the nozzle exit drops rapidly, reflecting the sharp rise in temperature and hence sound speed. The continued decrease in Mach number with distance must be interpreted to be a slowing down of the jet as it mixes with the still air around it in the test section. Deduced values must be taken with large uncertainty limits because of inherent uncertainties in the measurements.

§W. R. Warren, Jr., "Reacting Flow and Pressure Recovery Processes in HF/DF Chemical Lasers," presented at the Fourth International Colloquium on Gas Dynamics of Explosions and Reactive Systems, University of Calif., San Diego, Calif., July 10-13, 1973.

Conclusion

An approach in which combined experiments are used to determine certain important time-averaged, spatially averaged fluid properties of a reacting ($F+H_2$) supersonic free jet of a chemical laser is demonstrated. The effect of closed cavity HF lasing on this jet is discussed. The technique of using a rapid-scanning spectrograph to study the chemiluminescence is described.

Appendix

The spontaneous emission power per unit volume and solid angle from an isolated spectral line with width much less than instrument width is given by

$$P(v,J,\lambda) = \frac{hc}{4\pi\lambda}\eta A\bar{N}_v \Theta_v (2J+1)\exp\left[-\frac{J(J+1)\Theta}{T_R}\right] \times \frac{1}{\tau}\int_\tau \left[\frac{N_v(r)}{\bar{N}_v}\right]\left[\frac{T_R}{T(r)}\right] \times \left\{\exp\left[-\frac{J(J+1)\Theta_v}{T_R}\left(\frac{T_R}{T(r)}-1\right)\right]\right\} dr$$

where v and J are the vibrational and rotational quantum numbers and λ the wavelength. $A(v,J,\lambda)$ is the Einstein coefficient, Θ the characteristic rotational temperature, and η the transmission coefficient. Spatial variations in number density N_v and gas temperature T are considered. The averages of these over optical volume τ are $\bar{N}_v$ and T_R. It is clear that for uniform T in τ, the well-known analysis[5] for T_R will result regardless of nonuniformities in $N(r)$. The volume integral is unity. Generally, the integral measures the deviation of each spectral line power resulting from spatial nonuniformities in T from the straight line given by $\ln[\lambda P/A(2J+1)]$ vs $J(J+1)\Theta$. The exponential in the integrand is a dominant term at large J. The value of the integral, and therefore the deviation, then increases with J. The appearance is that of a concave upward distribution of spectral lines on the $J(J+1)\Theta$ graph when T is nonuniform in τ. The same trend can be generated when the independent variable is time instead of r.[10] The third possibility for a nonlinear behavior in $J(J+1)\Theta$ is a non-Boltzmann rotational distribution at large J.[11]

We examined a one-dimensional case of large density and small temperature variations:

$$N(z)/\bar{N} = 1 - \cos 2\pi z/L$$

$$T(z)/T_R = (1-\epsilon) + \epsilon(1-\cos 2\pi z/L)$$

where perturbation ϵ is 0.3. The computed values for the integral from $-L$ to $+L$ for $J=0$ to 10 are 0.887, 0.904, 0.941,

1.005, 1.109, 1.271, 1.521, 1.909, 2.518, 3.494, and 5.108. The average T_R is 280 K (so $\Delta T_R/T_R$ is 0.1); the apparent temperature deduced from the first five P-branch lines of HF $3\rightarrow0$ is 309 K. For $\pm30\%$ fluctuations in T, the deduced temperature is only 10% larger than T_R.

References

[1]Spencer, D. J., Mirels, H., and Durran, D. A., "Performance of CW HF Chemical Laser with H_2 or He Diluent," *Journal of Applied Physics*, Vol. 43, 1972, pp. 1151-1158.

[2]Kwok, M. A., Giedt, R. R., and Ueunten, R. H., "Development of the MESA Spectoscopy Experiment," TR-0074(4534)-3, The Aerospace Corp., El Segundo, Calif., Jan. 15, 1974, p. 44.

[3]Kwok, M. A., Giedt, R. R., and Varwig, R. L., "Selected Medium Diagnostics for a 10-kW CW HF Chemical Laser," TR-0075(5533)-1, The Aerospace Corp., El Segundo, Calif., Oct. 15, 1974, p. 53.

[4]Varwig, R. L. and Kwok, M. A., "CW HF Chemical Laser Flow Diagnostic Measurements," *AIAA Journal*, Vol. 12, Feb. 1974, pp. 208-212.

[5]Kwok, M. A., Spencer, D. J., and Gross, R. W. F., "Chemiluminescence from the Supersonic Jet of a CW HF Chemical Laser," *Journal of Applied Physics*, Vol. 45, Aug. 1974, pp. 3500-3506.

[6]Vasilev, G. K., Makarov, E. F., Ryabenko, A. G., and Talroze, V. L., "Rotational and Vibrational Deactivation of Excited HF Molecules," *Soviet Physics-JETP*, Vol. 41, April 1976, pp. 617-621.

[7]Wilkins, R. L., "Monte Carlo Calculations of Reaction Rates and Energy Distribution Among Reaction Products, I. $F+H_2\rightarrow HF+H$," *Journal of Chemical Physics*, Vol. 57, July 1972, pp. 912-917.

[8]Wilkins, R. L., "Monte Carlo Calculations of Reaction Rates and Energy Distribution Among Reaction Products, III. $H+F_2\rightarrow HF+F$ and $D+F_2\rightarrow DF+F$," *Journal of Chemical Physics*, Vol. 58, Mar. 1973, pp. 2326-2332.

[9]Varwig, R. L., "Photographic Observations of CW HF Chemical Laser Reacting Flow Field," *AIAA Journal*, Vol. 12, Oct. 1974, pp. 1448-1450.

[10]Lazdinis, S. S., "Effects of Fluctuations in Rotational Temperature, Vibrational Temperature, and Number Density on Time Averaged Electron Beam Measurement of Nitrogen Rotational Temperature," AIAA Paper 75-180, New York, 1975.

[11]Shackleford, W. L., Witte, A. B., Broadwell, J. E., Trost, J. E., and Jacobs, T. A., "Experimental Measurements in Supersonic Reacting $(F+H_2)$ Mixing Layers," *AIAA Journal*, Vol. 12, Aug. 1974, pp. 1009-1010.